Journal of Magnetic Resonance **137,** 221–230 (1999)
Article ID jmre.1998.1658, available online at http://www.idealibrary.com on IDEAL®

Pure Absorption Electron Spin Echo Envelope Modulation Spectra by Using the Filter-Diagonalization Method for Harmonic Inversion

Gunnar Jeschke,*[,1] Vladimir A. Mandelshtam,† and A. J. Shaka†

**Max-Planck-Institut für Polymerforschung, Postfach 3148, 55028 Mainz, Germany; and †Chemistry Department, University of California at Irvine, Irvine, California 92697*

Received August 19, 1998; revised November 13, 1998

Harmonic inversion of electron spin echo envelope (ESEEM) time-domain signals by filter diagonalization is investigated as an alternative to Fourier transformation. It is demonstrated that this method features enhanced resolution compared to Fourier-transform magnitude spectra, since it can eliminate dispersive contributions to the line shape, even if no linear phase correction is possible. Furthermore, instrumental artifacts can be easily removed from the spectra if they are narrow either in time or frequency domain. This applies to echo crossings that are only incompletely eliminated by phase cycling and to spurious spectrometer frequencies, respectively. The method is computationally efficient and numerically stable and does not require extensive parameter adjustments or advance knowledge of the number of spectral lines. Experiments on γ-irradiated methyl-α-D-glucopyranoside show that more information can be obtained from typical ESEEM time-domain signals by filter-diagonalization than by Fourier transformation.

Key Words: **pulse EPR; ESEEM; high resolution; filter-diagonalization method; linear prediction.**

INTRODUCTION

Electron spin echo envelope modulation (ESEEM) spectroscopy (*1–3*) is widely applied for structural characterization of paramagnetic centers in biological systems and materials (*4, 5*), as it surpasses electron paramagnetic resonance (EPR) spectroscopy in resolution for hyperfine-coupled nuclei. To obtain the spectrum from time-domain ESEEM signals, a frequency analysis must be performed. This analysis is usually done by Fourier transformation (FT) followed by calculation of a magnitude spectrum, thereby broadening spectral lines due to an admixture of dispersive line shape components. Recently, it has also been demonstrated that magnitude ESEEM spectra feature tremendous line shape distortions for the case of strongly overlapping lines (*6*). The calculation of better resolved pure absorption spectra, e.g., by phase correction, however, leads to intolerable baseline distortions for the usual situation of many spectral lines and relatively large dead times. Methods based on FT-based backprediction (*7*), linear prediction (*8, 9*), or FT-based iterative extraction of damped sinusoids from the time-domain signal (*10, 11*) have been proposed to overcome this problem. None of these approaches however seems to be sufficiently fast, reliable, and convenient for routine application.

Recently, a new method for high-resolution analysis of discrete time data was introduced (*12, 13*) that is based on the original filter diagonalization method (FDM) (*14*). Unlike the discrete FT, this method need not introduce any additional line broadening, even when the signal is measured for only a fraction of its decay time. That is, the usual boxcar multiplication in the time domain, and associated sinc function broadening in the frequency domain, properties well known in FT spectroscopy, need not apply to FDM analysis. Similarly to the FT, however, FDM features locality; i.e., it restricts spectral analysis to any desired small frequency domain. Because of this property the computational effort scales quasi-linearly with the number of data points as does the computational effort of FT. In contrast, the computational effort of linear prediction with, e.g., singular value decomposition (LPSVD) (*8*) scales with the third power of the number of points (or at least the number of assumed spectral features) and the latter method is also less computationally stable. Even when computation of LP coefficients is made efficient, the overall algorithm is still unacceptably slow for large numbers of spectral features (*15*). Furthermore, in contrast to LP, no initial estimate of the number of frequency components in the spectrum is required for FDM analysis. FDM can also be implemented in multiple time dimensions where the high resolution obtained for a small time window is of particular importance (*16*). Its potential for high-resolution analysis of 2D NMR data has been described recently (*17, 18*).

In the present context, it is of particular interest that FDM reliably and with few computational effort yields a list of frequencies, line widths, amplitudes, and phases. This list can be postprocessed using any additional information available about the system under study. In this work we demonstrate that this allows one to obtain pure absorption two-pulse (*1, 2*),

[1] To whom correspondence should be addressed. E-mail: jeschke@scientist.com.

1090-7807/99 $30.00

three-pulse (*2*), and four-pulse (*19–21*) ESEEM spectra that are significantly better resolved than magnitude spectra. In addition, artifacts due to spurious spectrometer frequencies and incompletely removed echo crossings can be easily eliminated from the spectra in most cases. The performance of FDM is compared to FT magnitude spectra for simulated data and for both a single crystal and powder sample of γ-irradiated methyl-α-D-glucopyranoside (*22*).

GENERAL CONSIDERATIONS

Features of ESEEM Time-Domain Signals

For a system consisting of an electron spin $S = \frac{1}{2}$ and N nuclear spins $I_i = \frac{1}{2}$ with anisotropic hyperfine couplings, the dependence of the two-pulse ESEEM signal on the interpulse delay τ disregarding relaxation is given by Mims' formula (*2*)

$$V_0(\tau) = \prod_l^N \left\{ 1 - \frac{k_l}{4} [2 - 2\cos(\omega_{l\alpha}\tau) - 2\cos(\omega_{l\beta}\tau) + \cos(\omega_{l+}\tau) + \cos(\omega_{l-}\tau)] \right\}, \quad [1]$$

where k_l is the modulation depth factor, $\omega_{l\alpha}$ and $\omega_{l\beta}$ are the nuclear frequencies in the electron spin α and β manifold, respectively, and ω_{l+} and ω_{l-} are their sums and differences, respectively. For electron spins $S > \frac{1}{2}$ a signal of the same general form is obtained for each of the observer transitions, only the calculation of the k_l and frequencies is slightly different (*23*). For nuclear spins $I > \frac{1}{2}$, the factors in the product are more complicated and no analytical formula can be given for a general case with significant nuclear quadrupole coupling. Note, however, that the factors still have the form of a sum of cosine functions with different amplitudes and signs.

Obviously, the spectrum of the time-domain signal described by Eq. [1] consists of lines in positive ($\omega_{l\alpha}$, $\omega_{l\beta}$) and negative (ω_{l+}, ω_{l-}) absorption with no dispersive part. Unfortunately, the signal cannot be measured for small τ because of a receiver dead time t_d after the second pulse of about 100 ns. With typical ESEEM frequencies in the range from 0 to 50 MHz, the phases of the single frequency components are usually distributed over the whole range from 0 to 2π after t_d. The simplest way to process such a signal is to redefine the time argument by $\tau' = \tau - t_d$ and to obtain a spectrum $S_0(\omega)$ by discrete complex FT of $V_0(\tau')$. A pure absorption spectrum $S'_0(\omega)$ can then be calculated by

$$S'_0(\omega) = \exp(i\omega t_d) S_0(\omega). \quad [2]$$

However, the situation changes if relaxation is taken into account. In a good approximation, the time-domain signal is given by

$$V(\tau') = \exp\left[-\frac{2(\tau' + t_d)}{T_m}\right] V_0(\tau'), \quad [3]$$

where T_m is the phase memory time of the electron spins that can be determined separately by a fit of the echo decay, since usually $k_l \ll 1$ for all l. In fact, this unmodulated part of the echo decay is removed before FT, since it would give rise to a very intense line at zero frequency otherwise. The effect of relaxation is a broadening of the spectral lines, while the phase at time t_d of the *whole* line with frequency ω_x is still given by $\varphi_x = \omega_x t_d$. The phase correction described by Eq. [2] is now certainly wrong for the "wings" of the line and thus works well only for isolated and sufficiently narrow lines and for short dead times. With typical values of T_m and t_d being in the order of 1 μs and 100 ns, respectively, lines often overlap and the "phase-corrected" spectra are heavily distorted. This problem is usually dealt with by computing the absolute value (or magnitude) spectrum from the result of the complex FT. In addition to broadening the lines by admixture of dispersive parts, this method still leads to distortions for overlapping lines, as has been demonstrated convincingly by Van Doorslaer *et al.* (*6*).

In principle, however, the correct spectrum can still be reconstructed from the time-domain data. After evaluating the product, Eq. [1] can be written in the form

$$V(\tau) = \sum_l^K d_l \cos(\omega_l \tau) \exp\left(-\frac{\tau}{T_{lm}}\right), \quad [4]$$

which is a special case of the harmonic inversion problem that corresponds to a fitting of a complex time signal by a sum of sinusoids. We can write

$$V(\tau) = \sum_l^K d_l \exp(-i\tau w_l), \quad [5]$$

with the unknown complex frequencies w_l and generally complex amplitudes d_l. The frequencies are then given by

$$w_l = \omega_l - \frac{i}{T_{lm}}. \quad [6]$$

Theoretically, if the number of data points in the signal $V(\tau)$ is greater than the number of unknowns, all unknowns can be determined by FDM and the original spectrum can thus be reconstructed perfectly. Equation [5] is a valid description of

the signal even if τ is replaced by $\tau' = \tau - t_d$. The w_l remain the same while the d_l are replaced by d'_l, which are no longer purely real. For a known or empirically determined dead time t_d, the original coefficients d_l can be recovered from the d'_l (*13*) by

$$d_l = \exp(iw_l t_d) d'_l. \qquad [7]$$

If the Lorentzian assumption of Eq. [5] is accurate, then Eq. [7] provides an exact phase correction, even if t_d is not small. Furthermore, it also corrects for the signal decay during the dead time.

These considerations can also be applied to other methods that accurately decompose the spectrum according to Eq. [5]. Note that the FT slicing algorithm introduced by Astashkin *et al.* fails to achieve such an accurate decomposition in the case of poorly resolved spectra, since the extracted damped sinusoids then feature systematic phase and damping errors (*10*). On the other hand, LPSVD (*8, 9*) can yield the required line lists, but is stable and sufficiently fast only if K is small and known. For unknown K, LPSVD is feasible only if all amplitudes have the same order of magnitude and are much larger than the noise level. In this case, a good guess for K can be obtained automatically or at least semi-automatically (*9*). Unfortunately, amplitude dynamics is usually large in ESEEM, as the k_l vary strongly. FDM, in contrast, does not require preliminary knowledge of K and can also be applied if K is large. If the number of poles (frequency–amplitude pairs) determined from the discrete time signal is larger than the number of spectral lines, the excessive solutions feature very small (ideally zero) amplitudes d_l. Spurious poles with significant amplitude are distinguished by either their large width or dependence on parameters of the FDM algorithm (*12*). They can often be easily rejected.

For three-pulse ESEEM with fixed interpulse delay τ between the first two pulses and variable interpulse delay T between the second and third pulse, the time-domain signal including relaxation is given by (*2, 24*)

$$\begin{aligned} E^{3p}(T) = \frac{1}{2}\exp\left(-\frac{2\tau}{T_m}\right)\Bigg\{ \prod_l^N \exp\left(-\frac{T}{T_{ln}}\right)\Bigg[1 - \frac{k_l}{2} \\ \times [1 - \cos(\omega_{l\alpha}\tau)][1 - \cos(\omega_{l\beta}(\tau + T))]\Bigg] \\ + \prod_l^N \exp\left(-\frac{T}{T_{ln}}\right)\Bigg[1 - \frac{k_l}{2}[1 - \cos(\omega_{l\beta}\tau)] \\ \times [1 - \cos(\omega_{l\alpha}(\tau + T))]\Bigg]\Bigg\}, \end{aligned} \qquad [8]$$

where the T_{ln} are the phase memory times of the nuclear spins. The signal is of a similar form as the one in two-pulse ESEEM and all considerations apply analogously. Note that the different frequency components are in phase at time $T = -\tau$, so that the dead time is given by $t_d^{3p} = T_0 + \tau$. Typical dead times in three-pulse ESEEM are therefore larger than those in two-pulse ESEEM. The problem of line shape and baseline distortions after FT is nevertheless somewhat diminished since only half as many frequency components appear for each nucleus and because the T_{ln} are considerably larger than T_m. However, a linear phase correction still usually fails to yield a useful spectrum. The problem of large amplitude dynamics and lines close to the noise level is aggravated by the blind spot behavior described by the factors $1 - \cos(\omega_{l\alpha})$ and $1 - \cos(\omega_{l\beta})$.

Another feature of ESEEM is that time-domain data must be sampled point-by-point. In this, the maximum dwell time d is limited by the Nyquist criterion $d < 1/(2\omega_{max})$, where ω_{max} is the maximum frequency expected to occur. Furthermore, with FT analysis, resolution is limited by the length of the time trace. To obtain ultimate resolution, especially in single crystal three-pulse ESEEM, one may then be forced to sample thousands of points. The problem is aggravated by the fact that this must be done for several τ values to overcome blind spot problems. With FDM analysis, on the other hand, the high resolution can be achieved with short time signals as long as the number of points is sufficient to represent the frequency components in the spectrum (*12, 16*).

So far, our discussion has assumed ideal microwave pulses, since Mims' formulas for two-pulse and three-pulse ESEEM are derived for this case. This assumption is usually a poor one in pulse EPR spectroscopy and it has been demonstrated that intensity deviations (*25*) as well as deviations from the product rule for two-pulse ESEEM (*26*) occur for typical experimental situations. Therefore, it may be suspected that also the linear dependence of phase on frequency may be violated. We find this indeed in our simulations of three-pulse ESEEM (see below) and will discuss this point in more detail elsewhere. Here it suffices to note that for a given line list, a pure absorption ersatz spectrum can be calculated even if the phases of single lines are arbitrary (*27*). In contrast, methods that only backpredict time domain data like LP *without* construction of the line list and Mims' method (*7*) cannot yield a pure absorption spectrum in such a situation.

Note, however, that this kind of phase correction should be applied with some caution. It works well if the spectrum is composed mainly of Lorentzian lines that do not overlap too strongly. Otherwise, harmonic inversion may model the shape of a single non-Lorentzian line or of a set of overlapping lines by a number of Lorentzian lines with different phases and amplitudes. The single components do not have any physical meaning and "correcting" their phases independently of each other would falsify line shape and amplitude.

Handling of the Noise and Artifacts

In addition to the signal from the spin system, experimental data contain white noise and sometimes instrumental artifacts. In general, such data can still be described by Eq. [4] but K will effectively be increased and the results of the harmonic inversion will slightly depend on the parameters of FDM. Any converged solution, however, will rather faithfully reproduce the frequency components with the largest amplitudes, so that one can still obtain a considerable part of the information on the spin system. The effects of noise on the solution are twofold. First, a number of poles will be obtained that serve to fit the noise; second, some error will be introduced into the parameters for the poles due to the spin system. The latter effect is also present if the parameters are determined by a line shape fit (deconvolution) after FT. It has been shown earlier that the errors for the spectral parameters determined by FDM is very small for sufficiently narrow spectral lines with good signal-to-noise ratio (*12*). Note that very broad spectral components are anyway suppressed in ESEEM, as their contribution to the signal decays completely within the relatively large dead time.

In the context of ESEEM spectroscopy, spectral lines and noise poles can often be distinguished on physical grounds. First, the dynamics of the spin system is purely dissipative; i.e., no frequency component should feature a negative width corresponding to an increase of modulation amplitude with time. Second, poles from the spin system with large widths will decay almost completely within the dead time. These two conditions alone usually suffice to reject most of the noise poles. In some cases, the range of possible widths is limited even further. For instance in two-pulse ESEEM, the line width of all signal components that arise from the spin system corresponds to T_{m}. Even if one allows for a generous error, only few noise poles match this condition for the line width. Even in three-pulse ESEEM, one can usually make a good guess for the reasonable range of the $T_{l\mathrm{n}}$. Furthermore, if a linear phase correction succeeds, noise poles can also be recognized by their arbitrary phase. This is another reason why linear phase correction should be preferred to phasing each frequency component separately whenever the former is possible.

These techniques for eliminating frequency components that do not arise from the spin system are not restricted to white noise. For instance, spurious frequencies introduced by the spectrometer itself also have arbitrary phase and do not decay at all. Another often encountered artifact in three-pulse ESEEM and experiments with even more pulses are echo crossings. Theoretically, echo crossings can be eliminated by phase cycling (*28*), but even with a well-adjusted spectrometer their suppression is not complete. As modulation depths are usually only in the order of a few percent of an echo signal, even small residual echo crossings may influence the outcome of an FT analysis. With FDM, echo crossings result in unphysically broad spurious lines, since they are confined to a narrow time interval typically much shorter than t_{d}. These artifacts can thus be eliminated from the line list before reconstruction of the spectrum.

Our discussion so far assumes that each spectral component from the spin system is represented by one pole in the FDM line list. For regions where lines overlap strongly or for significant deviations from Lorentzian lineshape, this may no longer be true. In such situations, one should consider carefully to which extent "unphysical" poles can be eliminated without falsifying lineshapes. Finally it should be noted that extensive elimination of noise poles from line lists can lead to apparently noiseless spectra. As one has come to expect that noise is fully represented in spectra, some care should be taken in the presentation of results to not mislead the casual observer. If preferred, the original noise can be restored for display as described earlier (*13*).

Disordered Systems

Much ESEEM work is done on disordered systems for which frequencies are distributed due to the anisotropy of hyperfine and nuclear quadrupole couplings. In principle, such spectra must be described by an infinite number of frequency components, so that FDM analysis seems not to be feasible. In practice, dead time and noise prevent a faithful reproduction of the original spectrum by *any* method, since contributions to the signal by broad regions of the powder line shape are inevitably lost. The observed modulations are due to the narrow components of the original spectrum, i.e., line shape singularities or transitions with only weak orientation dependence of the frequencies. In two-pulse ESEEM, the latter situation applies to the sum combinations ω_{l+} that are usually close to twice the nuclear Zeeman frequencies ω_{Il}. In three-pulse ESEEM, sum combinations do not occur, but they can be introduced by extending the experiment. In the so-called four-pulse ESEEM experiment introduced by Schweiger, a π pulse is inserted in the middle between the second and third pulse of a stimulated echo sequence, and the identical interpulse delays T between the π pulse and its neighboring $\pi/2$ pulses are incremented (*19, 20*). The formula for the echo modulation has been given by Tyryshkin *et al.* (*21*). Here it may suffice to note that it is of a similar general form as Eq. [1] and features blind spots that depend on both $\omega_{l\alpha}$ and $\omega_{l\beta}$. Again, the situation for data analysis is analogous to two-pulse ESEEM with the dead time for four-pulse ESEEM being $t_{\mathrm{d}}^{4\mathrm{p}} = T_0 + \tau/2$.

In any ESEEM experiment on a disordered system, the number of narrow frequency components surviving dead time is on the order of N like in ESEEM experiments on single crystals. In particular for sum peaks, the time domain signal may be quite closely approximated by Eq. [4] as relaxation is often the dominating broadening mechanism. For surviving singularities of other lines, model simulations show that they

can also be rather well approximated by a small number of Lorentzian lines. For these reasons, harmonic inversion by FDM may also be suitable for the analysis of ESEEM data from disordered systems as will be demonstrated below by experimental examples.

NUMERICAL SIMULATIONS

To test the general considerations, we have first performed numerical simulations based on both analytical ESEEM formulas and an implementation of density matrix formalism in MATLAB (*29*). In contrast to experiments, this approach allows us to control the degree of nonideality. As a model system we choose two protons with identical isotropic hyperfine couplings $a_{iso} = -1$ MHz both at a distance of 2.5 Å from the strictly localized electron spin. The two electron–proton axes include angles of 30 and 70° with the direction of the static field $\mathbf{B}_0$, respectively (see inset in Fig. 1a). For the static field we assumed $B_0 = 3500$ G corresponding to X-band frequencies and for the phase memory time $T_m = 2$ μs. Before FT analysis, time-domain data were apodized by a Hamming window and zero-filled to twice their original size throughout this paper. FDM analysis was performed in one step for the whole region of interest (0 to 35 or 0 to 40 MHz). The computation time for FDM on a DEC Alpha workstation ranged from 5 to 30 s depending on the number of data points in the ESEEM trace.

A theoretical two-pulse ESEEM time trace was calculated by means of Eqs. [1] and [3] and 0.5% white noise (with respect to the maximum echo amplitude) was added. The theoretical spectrum shown in Fig. 1a was obtained by a cosine FT of the data without assuming any dead time. When assuming a dead time $t_d = 100$ ns, a cosine FT leads to a strongly dephased spectrum (data not shown), and complex FT with calculation of a magnitude spectrum must be performed. In the resulting spectrum displayed in Fig. 1b, significant line broadening is found and some line shape distortion occurs in regions where spectral lines overlap. Furthermore, the amplitude sign information is lost.

If the same time domain data are analyzed with FDM, a linear phase correction according to Eq. [7] can be performed on the line list. The resulting spectrum is shown in Fig. 1c. It reproduces the theoretical spectrum quite nicely. All noise poles were retained in this case, except for those that are so broad that they could not have survived dead time if they were due to the spin system.

A three-pulse ESEEM time trace for the same system was simulated using density matrix formalism to consider the Hamiltonian of the spin system during microwave $\pi/2$ pulses of finite length $t_p = 16$ ns. For the fixed interpulse delay and the initial value of the variable delay we chose $\tau = 136$ ns and $T_0 = 112$ ns, respectively. A nuclear phase memory time of 5 μs was assumed for both protons. Again, a magnitude spectrum

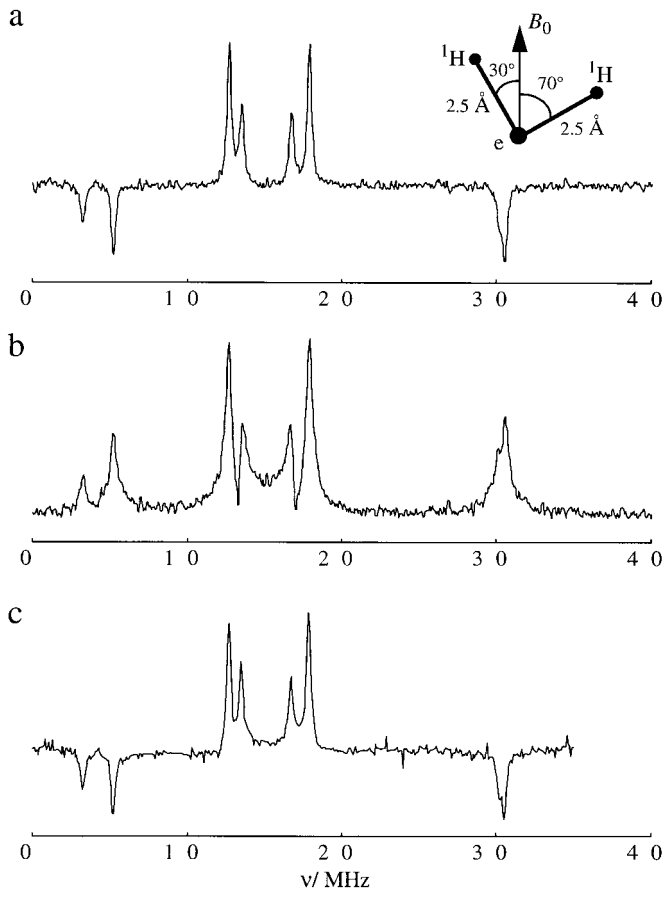

FIG. 1. Two-pulse ESEEM spectra (simulations) of a model system consisting of two protons hyperfine coupled to a localized electron spin. The isotropic hyperfine couplings are both −1 MHz. (a) Theoretical spectrum with noise added. The inset shows the geometry of the system. (b) FT magnitude spectrum assuming a dead time of 100 ns. (c) FDM pure absorption spectrum obtained from the same time domain data as in (b). Linear phase correction was applied.

must be computed after a complex FT to overcome phasing problems; the result is displayed in Fig. 2a. In addition to line broadening, we find a broad baseline artifact that can be traced back to an echo crossing that survives the four-pulse phase cycle introduced for three-pulse ESEEM by Fauth *et al.* (*30*). We tentatively assign this crossing to coherence transfer pathways that come into play only if microwave pulse nonideality is considered.

The spectrum obtained by FDM with subsequent linear phase correction is shown in Fig. 2b, it is obviously not properly phased. As closer examination reveals, this phase error is not due to a slight change in the effective t_d caused by the finite pulse widths. In fact, no linear phase correction with reasonable values for the constant- and frequency-dependent parameters is possible. Again we attribute this to effects of pulse nonideality. A detailed treatment is beyond the scope of this paper and will be published elsewhere. Despite this prob-

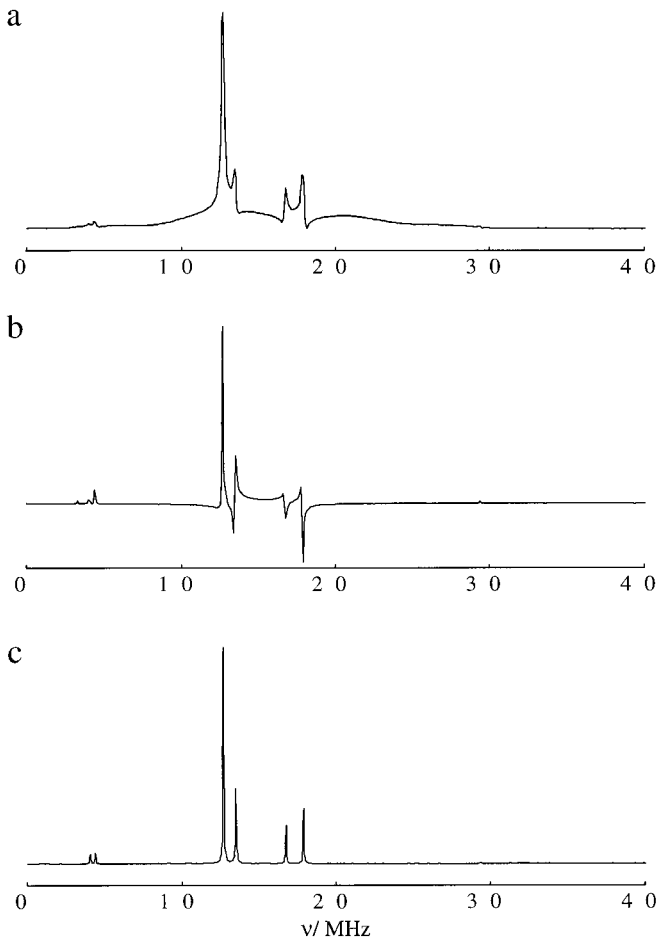

FIG. 2. Three-pulse ESEEM spectra (simulations) of the same model system as in Fig. 1. The corresponding time-domain data were simulated using density matrix formalism and assuming nonideal microwave pulses of 16 ns duration: (a) FT magnitude spectrum for $\tau = 136$, $T_0 = 112$ ns, (b) FDM spectrum obtained by applying linear phase correction corresponding to a dead time $t_d = \tau + T_0$, (c) FDM pure absorption spectrum obtained by phasing the single lines.

lem, a pure absorption ESEEM spectrum can be obtained by phasing each of the lines separately (see also (*27*)). The resulting FDM spectrum shown in Fig. 2c is again significantly better resolved than the FT magnitude spectrum. In addition, the broad baseline artifacts are eliminated as they correspond to unphysically broad contributions at the given t_d. The features at 4.06 and 4.39 MHz are difference combinations between lines of the two protons in the same electron spin manifold. Examination of the FDM peak list reveals that all the theoretical ESEEM frequencies are reproduced to a precision better than 2 kHz, despite the fact that the time trace is only 8.192 μs long. This demonstrates again the high-resolution character of FDM analysis (*12*) which allows one to avoid the tedious point-by-point sampling of very long time traces to obtain ultimate resolution.

In real systems, a much larger number of nuclei resides in the environment of an electron spin, most of them at a greater distance. To simulate this situation, we have randomly positioned 50 protons in space, assuming a normal distribution of the dipolar hyperfine couplings and an equal distribution of orientations of the electron–nuclear axes on a unit sphere. The complete list of parameters ($\omega_{I\alpha}$, $\omega_{I\beta}$, k_I) can be obtained from the authors at request. A two-pulse ESEEM time trace with 1024 data points was calculated by Eq. [1] using a dwell time of 8 ns and a dead time $t_d = T_0$

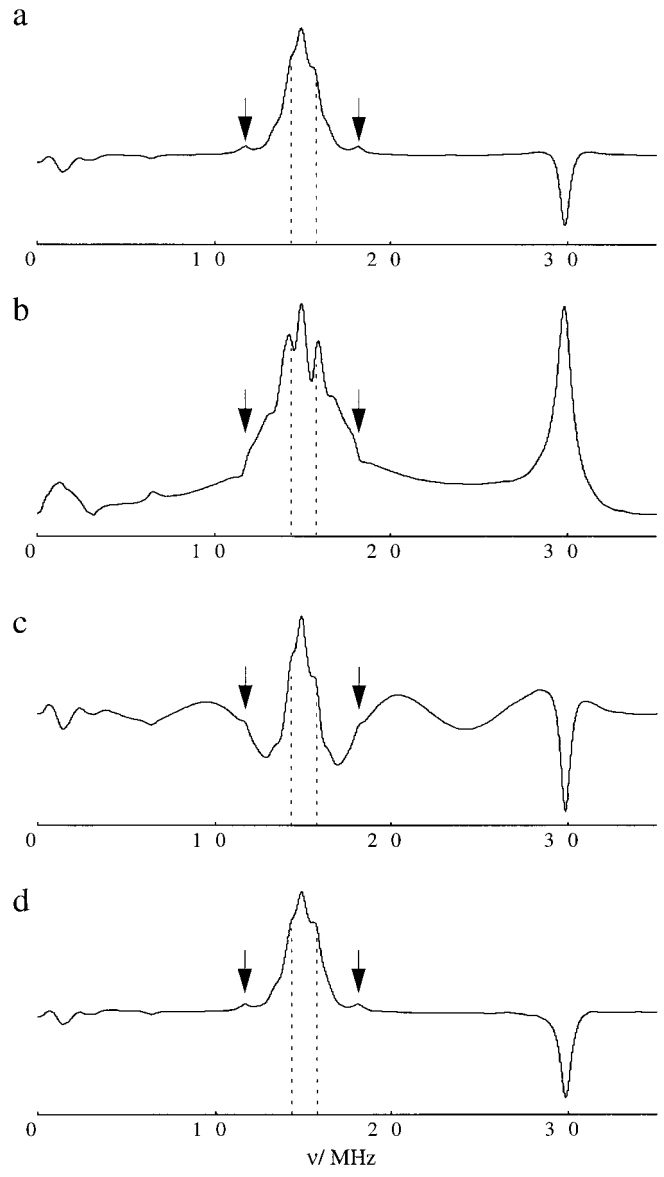

FIG. 3. Two-pulse ESEEM spectra of a system consisting of an electron spin and 50 protons (simulations). The arrows and dashed lines label a well and a partially resolved proton, respectively: (a) theoretical spectrum assuming $T_m = 1$ μs, (b) FT magnitude spectrum, (c) FT spectrum with linear phase correction, (d) FDM spectrum with linear phase correction.

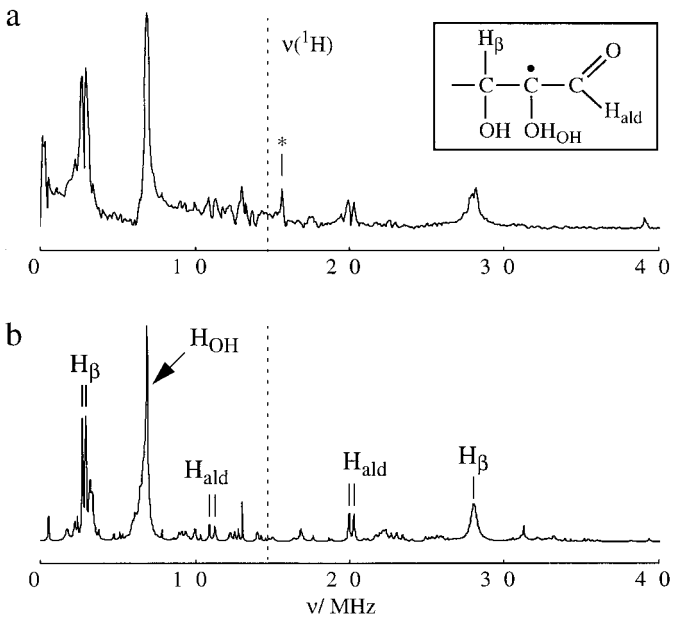

FIG. 4. Experimental three-pulse ESEEM spectra of γ-irradiated methyl-α-D-glucopyranoside with $\tau = 136$, $T_0 = 360$ ns. (a) FT magnitude spectrum. The peak labeled with an asterisk is a spurious frequency introduced by the spectrometer. The inset shows a fragment of the radical structure as proposed by Madden and Bernhard (*22*). (b) FDM pure absorption spectrum obtained from the same time-domain data as in (a). Single lines were phased and lines outside the line width range from 100 kHz to 2 MHz were rejected.

= 136 ns; the constant part was subtracted. This time trace overdetermines the 800 parameters of the basic, sum, and difference frequency lines of single protons, but underdetermines the problem including the combination frequencies between different protons. Furthermore, $T_m = 1$ μs was assumed. The theoretical spectrum is displayed in Fig. 3a.

The FT magnitude spectrum shown in Fig. 3b features a very broad background due to dispersive parts. Comparison to Fig. 3a reveals that a deconvolution of the magnitude spectrum would yield illusory couplings in addition to not revealing some real ones. Even the apparently well-resolved coupling of about 1.8 MHz is significantly wrong (see dashed lines). Note also the holes in the line shape marked by arrows, they correspond to peaks in the correct spectrum. The same phenomenon was observed in (*23*) and discussed in some detail in (*6*). As is demonstrated by the spectrum in Fig. 3c, this problem cannot be solved simply by applying Eq. [2] to the complex result of the FT. A baseline correction of this spectrum would be exceedingly difficult. FDM with linear phase correction, on the other hand, yields an absorption spectrum with undistorted baseline that agrees quite nicely with the theoretical one, as can be appreciated from Fig. 3d.

EXPERIMENTAL RESULTS

Methyl-α-D-glucopyranoside Single Crystal

Experimental tests were performed on samples of γ-irradiated methyl-α-D-glucopyranoside (α-MeGP). α-MeGP (>99%) was obtained from Fluka, single crystals were grown by slow evaporation from water and were γ-irradiated with a dosis of 30 kGy at room temperature. This gave rise to the same room temperature stable radical that was observed by Madden and Berhard after X-ray irradiation at 77 K and annealing (*22*). As a result of their ENDOR study, these authors proposed a structural fragment containing three protons with moderate to strong hyperfine couplings. A sketch of this fragment is displayed in the inset in Fig. 4a with the three protons under study labeled as H_β, H_{OH}, and H_{ald}. The principal values of the hyperfine tensors from (*22*) are reproduced in Table 1. Note that the values for H_{OH} are only estimates inferred from Madden and Bernhard's Fig. 7.

Three-pulse ESEEM data for different values of the interpulse delay τ were recorded at ambient temperature, at a static field $B_0 = 3445$ G, a microwave frequency $\nu_{mw} = 9.6485$ GHz, and at an arbitrary orientation of the crystal. The length of the $\pi/2$ pulses was 16 ns, and all measurements were performed using a Bruker ESP 380E spectrometer equipped with an EN 4118X-MD-4 ENDOR probe head. The time traces consist of 1024 data points with a dwell time of 8 ns. The FT magnitude spectrum for $\tau = 136$ ns and $T_0 = 360$ ns is displayed in Fig. 4a. For this τ value, protons with very small hyperfine couplings are largely suppressed by a blind spot. Nevertheless, the spectrum looks unexpectedly complicated and the resolution is rather poor, in particular in the region between 7 and 15 MHz. Note also that the peak at 15.625 MHz (labeled by the asterisk) is spurious and introduced by the spectrometer (one eights of the rate of the pulse controller).

Like in the three-pulse ESEEM simulation, linear phase correction using Eq. [7] after FDM analysis did not yield a pure absorption spectrum. Separate phasing of all poles (*27*) was used instead, and only spectral regions where not too many lines overlap too strongly are considered in the following. The FDM absorption spectrum displayed in Fig. 4b is significantly better

TABLE 1

Principal Values of the Hyperfine Tensors for Three Protons in the Room-Temperature Stable Radical Created by γ-irradiation of Methyl-α-D-glucopyranoside (from (*22*))

Proton	A_{11}/MHz	A_{22}/MHz	A_{33}/MHz
H_β	37.8	26.1	24.8
H_{OH}[a]	16	6	6
H_{ald}	6.1	3.0	2.3

[a] Values are estimated from Fig. 7 in (*22*).

resolved than the FT magnitude spectrum, which is in agreement with theoretical considerations and numerical simulations. In particular, the site splittings of the low-frequency line of the β protons and of the aldehyde protons can be determined more precisely. On the other hand, the high-frequency β proton line seems to exhibit more structure in the FT magnitude spectrum. We attribute this to artificially enhanced resolution by line shape distortions. However, this kind of resolution enhancement is not reliable, as can be inferred from (*6*) and has also been discussed above in connection with Fig. 3.

By removing components outside the line width range from 100 kHz to 2 MHz, we could get rid of the spectrometer artifact. The large number of unassigned features in the spectrum is only partially due to noise. Most of the features are actually combination lines between the lower nuclear frequencies of the β proton and other protons. This has been established by analysis of a HYSCORE (*31*) spectrum obtained under the same conditions and with the same value of τ (data not shown). The abundance of combination lines is due to the large modulation depth for the β protons which feature hyperfine couplings that approximately cancel the nuclear Zeeman energy in one of the electron spin manifolds.

Methyl-α-D-glucopyranoside Powder

For single crystals, three-pulse ESEEM is superior in resolution with respect to two-pulse ESEEM. However, this is not always the case for disordered systems where line broadening is dominated by the anistropy of interactions. Two-pulse ESEEM may then be preferable as it allows for smaller dead times and does not feature blind spots. A theoretical two-pulse ESEEM spectrum of α-MeGP has been calculated by using Eqs. [1] and [3], the hyperfine tensor principal values given in Table 1, and a phase memory time $T_m = 1$ μs; it is displayed in Fig. 5a. Powder averaging was performed for the single protons *before* applying the product rule, which is not strictly correct, but often the only way to go in practical situations. Otherwise the mutual orientation of all tensors must be known or fitted. The spectrum is dominated by contributions of the β proton because of its large modulation depth. Nevertheless some features from other protons can be clearly identified.

An experimental spectrum as obtained at $B_0 = 3445$ G and $\nu_{mw} = 9.6405$ GHz with pulse lengths of 16 and 32 ns for the $\pi/2$ and π pulse, respectively. The time trace consisted of 512 data points with a dwell time of 8 ns and a dead time of 136 ns. The situation in the experimental spectrum is somewhat more complicated than in the theoretical one because of the abundance of weakly coupled protons that contribute to a matrix line centered at the proton Zeeman frequency $\nu(^1H) = 14.67$ MHz. In fact, this line dominates the FT magnitude spectrum displayed in Fig. 5b and overshadows any other features in the region from about 10 to 19 MHz. Beside the matrix line, only the low-frequency line of the β protons can be assigned with any confidence in this spectrum.

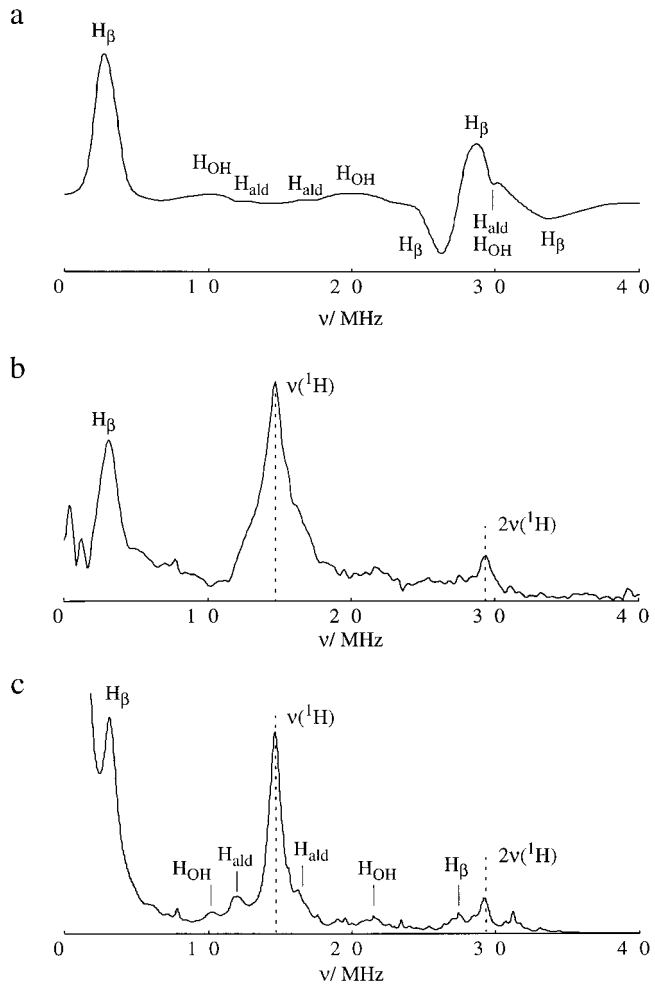

FIG. 5. Two-pulse ESEEM of γ-irradiated methyl-α-D-glucopyranoside. (a) Theoretical spectrum simulated using Mims' formula and the hyperfine tensor principal values given in Table 1. The labels assign features to the protons under study (see inset in Fig. 4a). (b) Experimental FT magnitude spectrum for $t_d = \tau_0 = 136$ ns. The proton nuclear Zeeman frequency $\nu(^1H)$ is marked. (c) FDM pure absorption spectrum obtained from the same time-domain data as in (b). The single lines were phased and lines outside the line width range from 100 kHz to 5 MHz were rejected. Assignments were checked by subjecting time-domain data corresponding to (a) to the same procedure.

A pure absorption spectrum was obtained again by using the FDM method and separately phasing the lines. The validity of such an approach is not obvious in this case, however, we have checked that it worked well with time domain data corresponding to the simulated spectrum. Contributions outside a line width range from 100 kHz to 5 MHz were eliminated. This FDM spectrum is much better resolved than the FT magnitude spectrum and allows one to assign a considerably larger number of features. The assignments were checked by subjecting time domain data corresponding to the theoretical spectrum to exactly the same analysis. The spectrum obtained (data not shown) is dominated by the low-frequency line of the β protons in the same way as the spectrum in Fig. 5a, suggesting that

this line is somewhat suppressed due to pulse nonideality in the experimental spectra. Note also that surviving spectral features do not always correspond to maxima or minima in the original spectrum. For instance the high-frequency feature of the OH protons corresponds to the edge of their spectral line. The described way of analyzing spectra via simulation, consideration of dead time, and the same method of data analysis as for experimental data may thus be mandatory for two-pulse ESEEM.

A more direct analysis may be possible for sum combinations ω_{I+} if these are properly resolved (*21, 32*). A simulation of the sum peak line shapes for the three protons under study reveals that the pseudosecular contributions are within the three-pulse ESEEM line width for the aldehyde proton and lead to strong broadening (line widths of several MHz) for the β proton. For the OH proton, the sum peak singularity is shifted by about 450 kHz with respect to $2\nu(^1\mathrm{H})$ as can be calculated from the values given in Table 1 and from the expressions given by Tyryshkin *et al.* (*21*). Given the line width in the pure absorption three-pulse ESEEM spectra of the single crystal, it should be possible to resolve this shift. To check this proposition, four-pulse ESEEM traces with 512 data points each, $T_0 = 304$ ns and a dwell time of 8 ns have been recorded at 32 different τ values from 104 to 352 ns. A four-step phase cycle like in three-pulse ESEEM was used. Otherwise the conditions were the same as in the two-pulse ESEEM experiment.

As the four-step phase cycle is incomplete for four-pulse ESEEM, an echo crossing appears in the time-domain data for $\tau = 280$ ns shown in Fig. 6a (see arrow). This results in tremendous spectral distortions in the range from 0 to 25 MHz in the FT magnitude spectrum displayed in Fig. 6b. Furthermore, spurious peaks are again observed at 15.625 and 31.25 MHz (labeled by asterisks). In the FDM spectrum in Fig. 6c, on the other hand, both types of artifacts are completely removed by rejecting frequency components with line widths outside the range from 300 kHz to 2.5 MHz. More significantly, the sum peak region (see insets in Figs. 6b and 6c) is much better resolved in the FDM spectrum as compared to the FT magnitude spectrum, and the sum peak of the OH protons shows up at the expected frequency marked by a dashed line.

Closer examination of the whole experimental data set shows that the OH proton sum peak can also be found in spectra at five other τ values (144, 192, 200, 208, 288 ns), while it is suppressed by blind spots in the rest of the traces. For the average frequency of the feature, we find $\nu_+(\mathrm{H_{OH}}) = 29.79 \pm 0.10$ in excellent agreement with the theoretical value of 29.8 MHz. In all the corresponding FT magnitude spectra, the feature can at best be recognized as a hole like in the inset in Fig. 6b. Sometimes it does not appear at all. Cross-term averaging as proposed for eliminating line shape distortions in magnitude spectra (*6*) is found to eliminate the hole but not to restore the peak. Indeed, the peak should not be resolved in an undistorted magnitude spectrum. We have also checked that

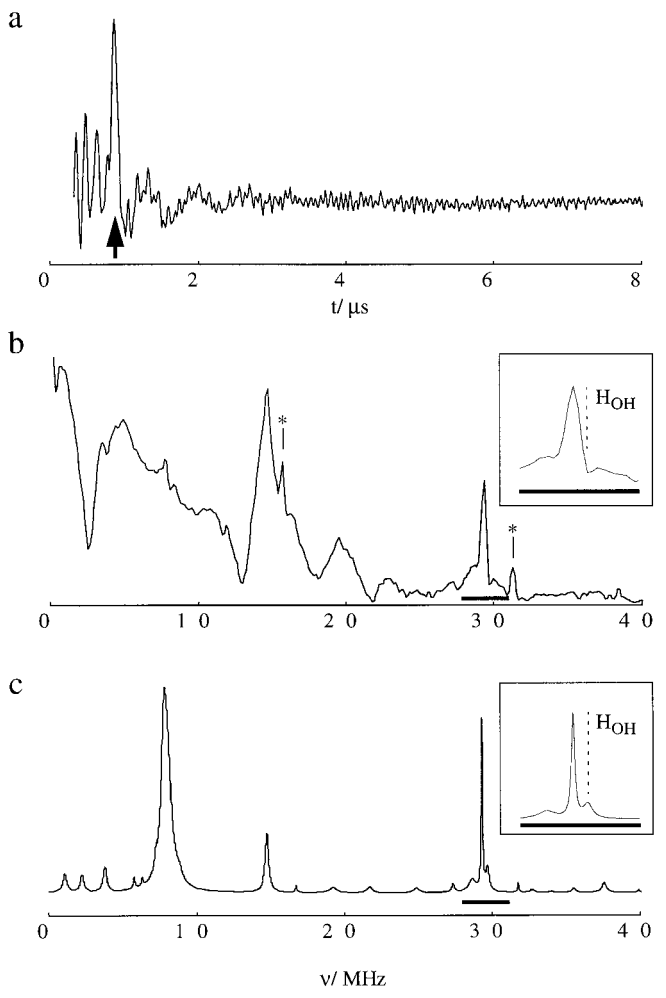

FIG. 6. Four-pulse ESEEM of γ-irradiated methyl-α-D-glucopyranoside with $\tau = 280$, $T_0 = 304$ ns. (a) Time-domain data. The arrow designates an echo crossing that has not been removed since an incomplete phase cycle was used deliberately. (b) FT magnitude spectrum of the time trace from (a). The asterisks label spurious peaks introduced by the spectrometer. The inset shows a magnification of the sum peak region with the dashed line labeling the frequency where the OH proton feature is expected. (c) FDM pure absorption spectrum of the time trace from (a) (single lines phased, lines with widths outside the range from 300 kHz to 2.5 MHz rejected). The inset again shows a magnification of the sum peak region which is now much better resolved and reveals the expected feature.

the feature is still unresolved in FT magnitude spectra if a proper phase cycle is used or more data points are recorded. Analysis of the data by calculating a 2D FT magnitude spectrum (*20*) reveals the feature if extensive zero filling is used. However, the frequency determined by the latter method is less precise (29.95 ± 0.20 MHz).

CONCLUSION

Harmonic inversion by the filter diagonalization method has several advantages over Fourier transformation in ESEEM data

analysis. By using information on the expected line widths, artifacts due to both incompletely removed echo crossings and spurious spectrometer frequencies can be removed from the spectra. The most significant advantage, however, is a considerable increase in resolution that is due to the elimination of dispersive contributions from the ESEEM spectra. Such an FDM reconstruction of pure absorption ESEEM spectra can be done reliably for long dead times, a large number of frequency components, and even in cases where the dependence of phase on frequency is nonlinear. FDM data analysis has the potential for becoming a routine method since it is fast and stable and does not require more user effort than FT data analysis. We expect that this new tool will enhance the versatility of ESEEM methods for structure determination by retrieving more information from given experimental data.

ACKNOWLEDGMENTS

We thank A. Sammet, D. Hessinger, and W. Lämmler for sample preparation. Communication of a manuscript (*6*) prior to publication by S. Van Doorslaer, G. A. Sierra, and A. Schweiger is gratefully acknowledged. A.J.S. acknowledges the National Science Foundation, Grant CHE-9625674.

REFERENCES

1. L. G. Rowan, E. L. Hahn, and W. B. Mims, *Phys. Rev. A* **137,** 61 (1965).
2. W. B. Mims, *Phys. Rev. B* **5,** 2409 (1972).
3. S. A. Dikanov and Yu. D. Tsvetkov, "Electron Spin Echo Envelope Modulation (ESEEM) Spectroscopy," CRC Press, Boca Raton (1992).
4. V. J. DeRose and B. M. Hoffmann, *Methods Enzymol.* **246,** 554 (1995).
5. L. Kevan, *Accounts Chem. Res.* **20,** 1 (1987).
6. S. Van Doorslaer, G. A. Sierra, and A. Schweiger, *J. Magn. Reson.,* in press.
7. W. B. Mims, *J. Magn. Reson.* **59,** 291 (1984).
8. H. Barkhuijsen, R. de Beer, W. M. M. J. Bovée, and D. van Ormondt, *J. Magn. Reson.* **61,** 465 (1985).
9. R. de Beer and D. van Ormondt *in* "Advanced EPR. Applications in Biology and Biochemistry" (A. J. Hoff, Ed.), Chap. 4, Elsevier, Amsterdam (1989).
10. A. V. Astashkin and A. Kawamori, *J. Magn. Reson. A* **112,** 24 (1995).
11. A. V. Astashkin, A. Kawamori, Y. Kodera, S. Kuroiwa, and K. Akabori, *J. Chem. Phys.* **102,** 5583 (1995).
12. V. A. Mandelshtam and H. S. Taylor, *J. Chem. Phys.* **107,** 6756 (1997).
13. H. Hu, Q. N. Van, V. A. Mandelshtam, and A. J. Shaka, *J. Magn. Reson.* **134,** 76 (1998).
14. M. R. Wall and D. Neuhauser, *J. Chem. Phys.* **102,** 8011 (1995).
15. H. Gesmar and P. C. Hansen, *J. Magn. Reson. A* **106,** 236 (1994).
16. V. A. Mandelshtam and H. S. Taylor, *J. Chem. Phys.* **108,** 9970 (1998).
17. V. A. Mandelshtam, H. H. Hu, and A. J. Shaka, *Magn. Reson. Chem.* **36,** S11 (1998).
18. V. A. Mandelshtam, H. S. Taylor, and A. J. Shaka, *J. Magn. Reson.* **133,** 304 (1998).
19. A. Schweiger, *Angew. Chem. Int. Ed. Engl.* **30,** 265 (1991).
20. S. Van Doorslaer and A. Schweiger, *Chem. Phys. Lett.* **281,** 297 (1997).
21. A. M. Tyryshkin, S. A. Dikanov, and D. Goldfarb, *J. Magn. Reson. A* **105,** 271 (1993).
22. K. P. Madden and W. A. Bernhard, *J. Phys. Chem.* **84,** 1712 (1984).
23. G. Jeschke and A. Schweiger, *J. Chem. Phys.* **106,** 9979 (1997).
24. S. A. Dikanov, A. A. Shubin, and V. N. Parmon, *J. Magn. Reson.* **42,** 474 (1981).
25. G. Jeschke and A. Schweiger, *Molec. Phys.* **88,** 355 (1996).
26. G. Jeschke and A. Schweiger, *J. Chem. Phys.* **105,** 2199 (1996).
27. Yung-Ya Lin, P. Hodgkinson, M. Ernst, and A. Pines, *J. Magn. Reson.* **128,** 30 (1997).
28. C. Gemperle, A. Aebli, A. Schweiger, and R. R. Ernst, *J. Magn. Reson.* **88,** 241 (1990).
29. "The Math," Works, Inc., Natick, MA.
30. J.-M. Fauth, A. Schweiger, L. Braunschweiler, J. Forrer, and R. R. Ernst, *J. Magn. Reson.* **66,** 74 (1986).
31. P. Höfer, A. Grupp, H. Nebenführ, and M. Mehring, *Chem. Phys. Lett.* **132,** 279 (1986).
32. A. Schweiger, *in* "Modern Pulsed and Continuous-Wave Electron Spin Resonance" (L. Kevan and M. K. Bowman, Eds.), Chap. 2, Wiley, New York (1990).